



Kinematics and dynamics of pedestrian head ground contact: A cadaver study

Shi Shang, Catherine Masson, David Teeling, Max Py, Quentin Ferrand,
Pierre-Jean Arnoux, Ciaran Simms

► To cite this version:

Shi Shang, Catherine Masson, David Teeling, Max Py, Quentin Ferrand, et al.. Kinematics and dynamics of pedestrian head ground contact: A cadaver study. Safety Science, 2020, 127, pp.104684. 10.1016/j.ssci.2020.104684 . hal-03228376

HAL Id: hal-03228376

<https://amu.hal.science/hal-03228376>

Submitted on 18 May 2021

HAL is a multi-disciplinary open access archive for the deposit and dissemination of scientific research documents, whether they are published or not. The documents may come from teaching and research institutions in France or abroad, or from public or private research centers.

L'archive ouverte pluridisciplinaire **HAL**, est destinée au dépôt et à la diffusion de documents scientifiques de niveau recherche, publiés ou non, émanant des établissements d'enseignement et de recherche français ou étrangers, des laboratoires publics ou privés.



Distributed under a Creative Commons Attribution - NonCommercial - NoDerivatives 4.0
International License

Kinematics and dynamics of pedestrian head ground contact: a cadaver study

Shi Shang¹, Catherine Masson², David Teeling¹, Max Py², Quentin Ferrand², Pierre-Jean Arnoux²,
Ciaran Simms^{1*}

¹ Trinity Centre for Bioengineering, Trinity College Dublin, Ireland

² Laboratoire de Biomécanique Appliquée (IFSTTAR – Université de la Méditerranée), France

*Corresponding Author (Email: csimms@tcd.ie)

Abstract

Pedestrians struck by vehicles are generally injured by the primary vehicle contact but also the secondary ground contact. However, experimental evidence for ground contact injuries is limited. Here we report on six staged cadaver tests at 20-30km/h with passenger cars/vans in which we recorded the whole process from first pedestrian contact until after the end of the ground contact is complete using high-speed video and accelerometers mounted in the cadavers. Results show distinct phases for pedestrian flight and ground contact in addition to the already established vehicle contact phases. No skull fractures were observed in any of the tests. However, for the speed range tested, the linear and angular head injury risk (evaluated using HIC/3ms & BrIC respectively) is generally higher from the ground contact compared to the vehicle contact. Although not yet clearly understood, angular head injury risk during ground contact is higher for the 20km/h tests compared to the 30km/h tests. A good comparison was observed with respect to previously predicted ground contact mechanisms and head impact speeds from multibody modelling. These results emphasize the importance of ground related injuries to pedestrians when struck by vehicles at speeds of 20-30km/h and provide a unique dataset for computational model validation of pedestrian ground contact.

Keywords

Pedestrians, vehicle contact, ground contact, cadaver test analysis

1. Introduction

The World Health Organization reports nearly 300,000 pedestrian fatalities annually (WHO, 2013), with many more injured. Injuries occur during the primary vehicle contact and, following separation from the vehicle, significant additional injuries often occur during ground contact. In early collision reconstruction work, Ashton and Mackay (Ashton and Mackay, 1983) showed that for vehicle impact speeds below about 25km/h, ground contact injuries exceed those of vehicle contact, but at higher speeds injuries from vehicle contacts predominate.

Pedestrian injuries in contacts with vehicles are generally well understood, with vehicle speed/shape/stiffness and pedestrian age/height/stance all influencing injury outcome (Kalra et al., 2016; Li et al., 2017a; Li et al., 2017b; Niebuhr et al., 2016; Rosen et al., 2011; Shang et al., 2018b; Simms, 2005; Simms and Wood, 2009). However, pedestrian ground contact involves a wide range of contact orientations and a complex combination of slide, roll and bounce to rest. The resultant injury mechanisms are not well understood as significant challenges persist in predicting the kinematics of this long timeframe event and in attributing injuries observed to either vehicle or ground contact (Simms and Wood, 2009). However, recent analysis of the German collision database GIDAS showed that the head, thorax and spine dominate AIS4-5 ground contact injuries,

and ground contact injury severity increases with pedestrian age and vehicle speed (Shang et al., 2018b). For collisions below 40 km/h, about two thirds of pedestrian injury costs were attributed to ground contact, emphasising the importance of ground contact injuries for low impact speeds (Shang et al., 2018b). Badeo-Romero and Lenard assessed UK collisions and also found a significant role for ground contact (Badea-Romero and Lenard, 2013).

Of particular interest is the manner in which pedestrian ground contact injuries are influenced by vehicle speed and design in the speed range 20-40 km/h, since this could lead to vehicle-based methods to reduce the severity of ground contact injuries in cases where pedestrian injuries from vehicle contact are mostly survivable. Computational modelling studies have posited various relationships between vehicle shape and ground contact injuries (Crocetta et al., 2015; Gupta et al., 2015; Gupta and Yang, 2013; Kendall et al., 2006; Tamura and Duma, 2011; Tamura et al., 2014; Xu et al., 2016). In particular, Crocetta et al. (Crocetta et al., 2015) reported on six identifiable ground contact “mechanisms” distinguished by the amount of whole body rotation of the pedestrian prior to ground contact, with average head impact speed varying between the different mechanisms. Some support for identifying an influence of vehicle design on pedestrian ground contact was found by Shang et al (Shang et al., 2018b) who used collision data to show that the normalised bonnet leading-edge height (bonnet height/hip height) is a risk factor for adult pedestrian AIS2+ ground-related head injuries. Further, Han et al. (Han et al., 2018) found from video analysis of real-world collisions that vehicle front shape and impact speed both influence ground contact kinematics. However, no pedestrian models are validated for ground contact and establishing initial conditions and injury outcomes in real world video cases is challenging.

Cadaver tests provide model validation data and have the potential to greatly strengthen our understanding of pedestrian ground contact. However, previous tests have mainly focused on vehicle contact, with limited reference to ground contact (Kerrigan et al., 2007; Masson et al., 2007; Paas et al., 2015; Subit et al., 2008) or else crash test dummies were used (Hamacher et al., 2011; Taneda et al., 1973). In early work, (Cavallero et al., 1983) concluded that head-ground contact location and speed could not be predicted from vehicle shape. However, tests were performed only at 32 km/h, vehicle shapes have changed substantially and no ground contact kinematics or injuries were reported. More recently, cadaver studies performed in the US and France have used a range of vehicle shapes and pedestrian sizes (Kerrigan et al., 2007; Paas et al., 2015; Subit et al., 2008), but ground contact kinematics/injuries were not evaluated. In fact, the sequence of pedestrian motion following head contact on vehicle has received little attention and is poorly described.

In summary, pedestrian ground contact kinematics remain poorly understood. Model predictions of ground contact mechanisms have been presented, but validation is lacking. Real-world collisions show the importance of ground contact, but the role of vehicle design in mediating pedestrian ground contact injury remains uncertain and existing cadaver data is limited. Accordingly, the aims of the current study are to:

- 1) perform staged vehicle impact tests using cadavers to study the kinematic chain of events in a pedestrian collision, starting with first vehicle contact and ending after the pedestrian strikes the ground.
- 2) assess pedestrian post-impact kinematics as well as head ground contact, including linear and rotational components of head injury risk.
- 3) assess potential interactive effects of vehicle speed and normalised bonnet leading edge height on pedestrian head injury risk during ground contact.

2.Methods

2.1 Cadaver Test Setup

As part of the Faculty of Medicine of Marseille, the Laboratory of Applied Biomechanics is enabled to perform full body human testing from body donations. Six cadaver tests were conducted to study pedestrian ground contact at Aix-Marseille Université: Faculté de Médecine-secteur Nord Marseille, see Table 1. Winckler's preparation (Winckler, 1974) or zinc chloride (Goodarzi et al., 2017) was used for tissue preservation. For each subject, up to 54 anthropometric measures were performed, and the external anthropometries are listed in Appendix A. The study was approved by the Ethical Committee of Aix-Marseille University. Three vehicle types (Appendix B) were tested to achieve different normalized bonnet leading edge heights (NBLEH), and each vehicle type was tested twice under similar conditions (different cadavers but approximately the same initial stance). Damaged vehicle components were replaced as necessary. The expected ground contact "mechanism" (Appendix C) based on the simulation study by Crocetta et al (Crocetta et al., 2015) for each case is also shown. Five 1000 fps cameras captured the whole pedestrian trajectory (Appendix D). Impact speeds of 20 or 30km/h were applied.

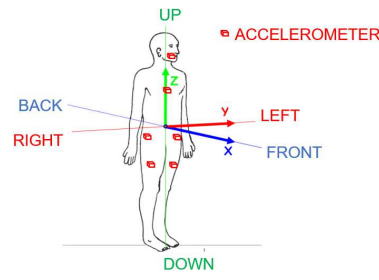
Table 1: Summary of tests performed

Test number	Vehicle speed (km/h)	Pedestrian/ vehicle size	NBLEH	Expected mechanism (M1-M6) (Crocetta et al., 2015) – see Appendix C
Test 01	30.5	Peugeot 307 (sedan) + (Male, 88 y/o, 1.74m, 66kg)	0.7	M1 (most frequent) or M3 (less frequent) mechanism for adults struck by compact car at 30 kph – Figure 8 in (Crocetta et al., 2015)
Test 02	30.4	Peugeot 307 (sedan) + (Male, 83 y/o, 1.72m, 69kg)	0.7	
Test 03	20.4	Citroen C4 (compact)+ (Male, 94 y/o, 1.67m, 64kg)	0.9	M2 (most frequent mechanism for adults struck by any vehicle at 20 kph) - Figure 7 in (Crocetta et al., 2015)
Test 04	21.0	Citroen C4 (compact)+ (Male, 83 y/o, 1.67m, 55kg)	0.9	
Test 05	30.1	Renault Kangoo II (van)+ (Female, 94 y/o, 1.58m, 38kg)	1.2	M2 (most frequent) or M1 (less frequent) mechanism for adults struck by a Van at 30 kph) - Figure 8 in (Crocetta et al., 2015)
Test 06	30.4	Renault Kangoo II (van)+ (Male, 86 y/o, 1.62m, 69kg)	1.1	

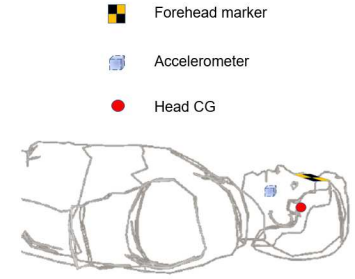
The cadavers were held by a magnetic locking system which automatically released just before vehicle contact, see Figure 1a. Fiducial markers recorded landmark positions on the head, extremities, pelvis and chest. The approximate initial lower extremity joint angles are shown in Appendix E. Full braking ($\mu \approx 0.8$) was applied after first pedestrian contact. Six triaxial accelerometers (10 kHz sample rate, -3dB AA hardware filter) were inserted in the cadavers (see Figure 1b): one was inserted in the chest, two were screwed on the left and right thigh bones, two were inserted in the ilium (left and right side) and one was inserted in the mouth to represent an approximate head CG. The mouth accelerometer was pressed against the palate and expanding foam was used to fill the mouth cavity. The accelerometer position was maintained during setting and curing. When dry, the surplus was removed and the head was equipped with a hood. Only the head accelerometer data is presented in this paper.



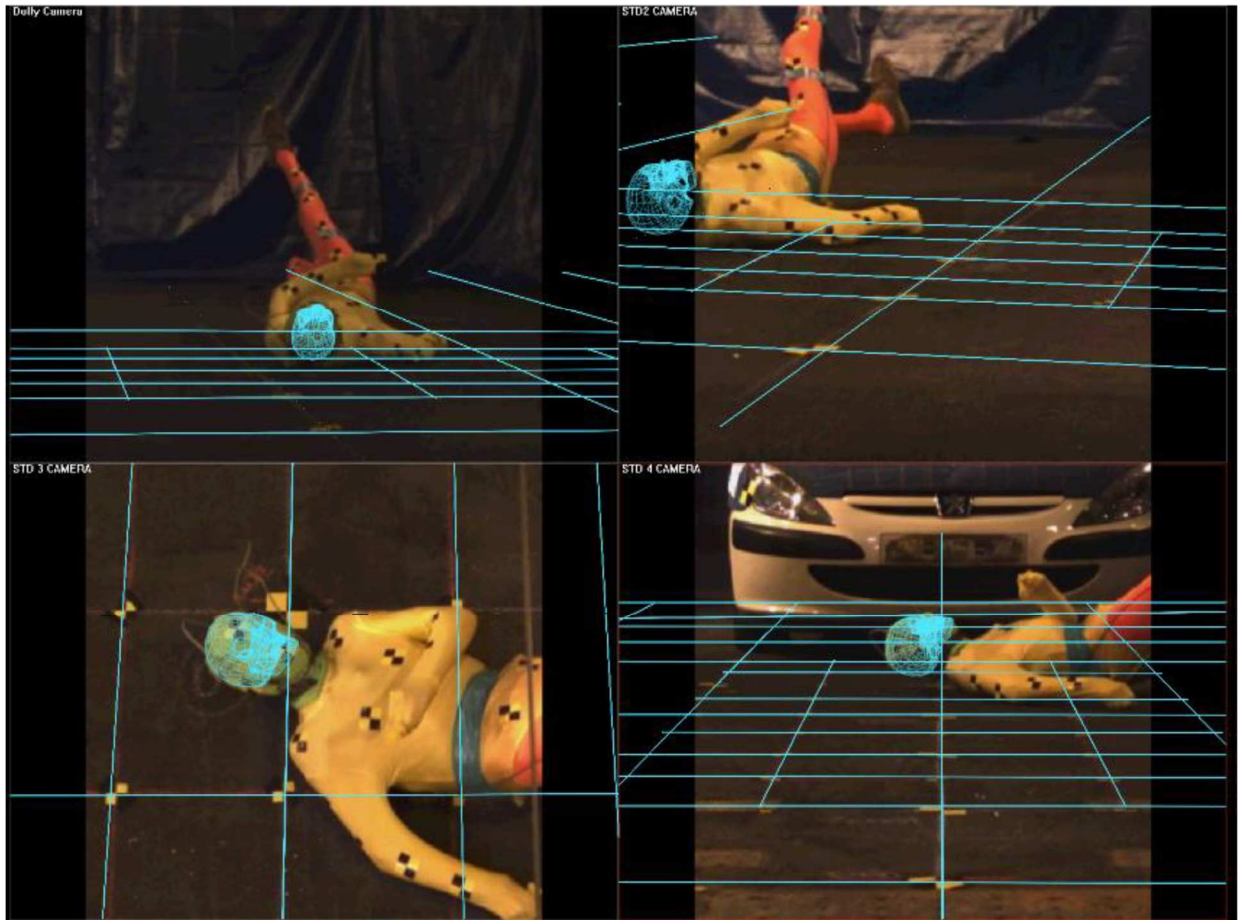
(a)



(b)



(c)



(d)

Figure 1: (a) Pre-impact scenario; (b) accelerometer positions and nominal orientations; (c) head accelerometer, CG and forehead marker positions; (d) Sample head MBIM matching using multi-view camera images

2.2 Video Data Analysis

Head trajectories in the X (vehicle forward direction) and Z (vertically upward) directions were estimated by manually tracking the location of the forehead marker (Figure 1c) every 10ms (or every 1ms during head contacts). Linear velocities were obtained using a central difference scheme. Rotational kinematics for the head during both vehicle and ground contacts were estimated using Model Based Image Matching (MBIM), introduced by (Bahr and Krosshaug, 2005) and recently applied to head impacts (Tierney et al., 2015; Tierney et al., 2018). MBIM uses multiple camera

views to build an environment based on known background dimensions. The user manually fitted a skull model (from the Poser platform) to the envelope of the head from videos at each time frame (1ms), see Figure 1(d). The rotation matrix for the head was then extracted at each time step, and a central difference scheme was used to compute body local angular velocity components. Each case was reconstructed by two independent researchers. Tierney et al (Tierney et al., 2018) previously reported that MBIM is repeatable for both single and multiple researchers.

2.3 Head injury assessments

The Head Injury Criterion (*HIC*) is commonly used to assess skull fracture risk (Hutchinson et al., 1998; Versace, 1971):

$$HIC = \left\{ \left[\frac{1}{t_2 - t_1} \int_{t_1}^{t_2} a_m(t) dt \right]^{2.5} (t_2 - t_1) \right\}_{max},$$

where t_1 and t_2 are initial/final times (in seconds) to maximize *HIC*, and a_m is the resultant head CG acceleration (units of g), with time duration ($t_2 - t_1$) constrained to be less than 15 ms. However, since our accelerometers were fixed in the mouth instead of the head CG (Figure 1c) for practical reasons, strict computation of *HIC* was not possible with our available instrumentation. Instead, we define the “approximate Head Injury Criterion” (*aHIC*), calculated by applying the *HIC* computation to our head accelerometer data. To verify this approach, a virtual sensor was inserted in the same location in the 50th percentile male MADYMO pedestrian model to check the difference between *HIC* and *aHIC* in a simulation similar to those in (Shang et al., 2018a). Results showed an approximate 10% difference, suggesting this approach is reasonable. The reported threshold for *HIC* is 700 for an approximate 30% chance of skull fracture (Schmitt et al., 2010). The 3ms acceleration criterion for the head was also calculated, used in regulations (ECE, 2008, 2010) to assess energy dissipation in a vehicle, and it requires that accelerations of duration greater than 3ms do not exceed 80g (Got et al., 1978).

To assess the risk of rotationally induced brain injuries, the Brain Injury Criterion (*BrIC*) (Takhounts et al., 2013) during vehicle and ground contact was assessed using the MBIM results. The *BrIC* is associated with traumatic brain injuries (TBI), which has been used to assess the brain injuries of vulnerable road users (Gabler et al., 2016; Gabler et al., 2018; Kimpara and Iwamoto, 2012; Mueller et al., 2015) and athletes (Aomura et al., 2016). (Gabler et al., 2018) also proposed another criterion, UBrIC, to assess rotationally induced brain injury. However, evaluation of UBrIC requires a measure of angular acceleration which could not be reliably predicted with the available equipment. The *BrIC* score is found from the peak body local head angular velocities:

$$BrIC = \sqrt{\left(\frac{\omega_x}{\omega_{xc}} \right)^2 + \left(\frac{\omega_y}{\omega_{yc}} \right)^2 + \left(\frac{\omega_z}{\omega_{zc}} \right)^2},$$

where ω_x , ω_y and ω_z are the peak head angular velocity components and $\omega_{xc} = 66.3rad/s$, $\omega_{yc} = 56.5rad/s$, $\omega_{zc} = 42.9rad/s$ are critical values proposed by Takhounts et al (Takhounts et al., 2013). The *BrIC* score was used to estimate the risk of an AIS3+ brain injury (Takhounts et al., 2013) in this study.

3.Results

3.1 Pedestrian kinematics during the whole process of vehicle impact

Figure 2 and Table 2 summarize overall kinematics, impact timings and intervals of the impact phases, with timings determined from the head accelerometer. Establishing the approximate contact time interval for both head-to-vehicle and head-to-ground contact in all tests was achieved by a combination of the filtered accelerometer and video data. For the onset of contact a sharp change in the accelerometer time curve could be readily identified in each case and verified by comparison with the video data. Establishing the effective end time for each contact was more challenging and no general criterion could be applied. Instead the end time was estimated by inspecting the acceleration time-history and comparing this to the video data. The time of first contact between the vehicle and pedestrian is t_0 . The pedestrian rotates onto the bonnet during phase 1. The time of first head impact on vehicle is t_1 . The pedestrian moves with the vehicle in phase 2. At t_2 , the pedestrian separates from the vehicle due to braking. The pedestrian has a flight period (phase 3) until t_3 , when first ground contact occurs (any body part). Then t_4 is the time of first head ground contact (in some cases $t_4 = t_3$). There follows a period of slide/roll and bounce (phase 4) until the pedestrian becomes stationary at t_5 . Appendix F shows the pedestrian head trajectories in the X (horizontal) and Z (vertical) directions for all six tests. Head impact locations on the vehicle are shown in Appendix G.

Table 2: Key vehicle and ground contact events (s)

Key time	t_0	Phase 1 duration	t_1	Phase 2 duration	t_2	Phase 3 duration	t_3	t_4	Phase 4 duration	t_5
Description	1 st vehicle pedestrian contact		1 st head vehicle contact		pedestrian & vehicle separate		1 st ground contact (any)	1 st head ground contact		Pedestrian at rest
Test 01 (30.5 kph)	0	0.145	0.145	0.625	0.770	0.203	0.973	0.995	1.270	2.265
Test 02 (30.4 kph)	0	0.153	0.153	0.557	0.710	0.276	0.986	0.986	1.019	2.005
Test 03 (20.4 kph)	0	-	none	-	0.834	0.195	1.029	1.180	1.303	2.483
Test 04 (21 kph)	0	0.169	0.169	0.571	0.740	0.185	0.905	0.970	1.824	2.794
Test 05 (30.1 kph)	0	0.098	0.098	0.549	0.647	0.213	0.86	0.860	1.374	2.234
Test 06 (30.4 kph)	0	0.110	0.110	0.617	0.727	0.202	0.929	0.936	1.193	2.129

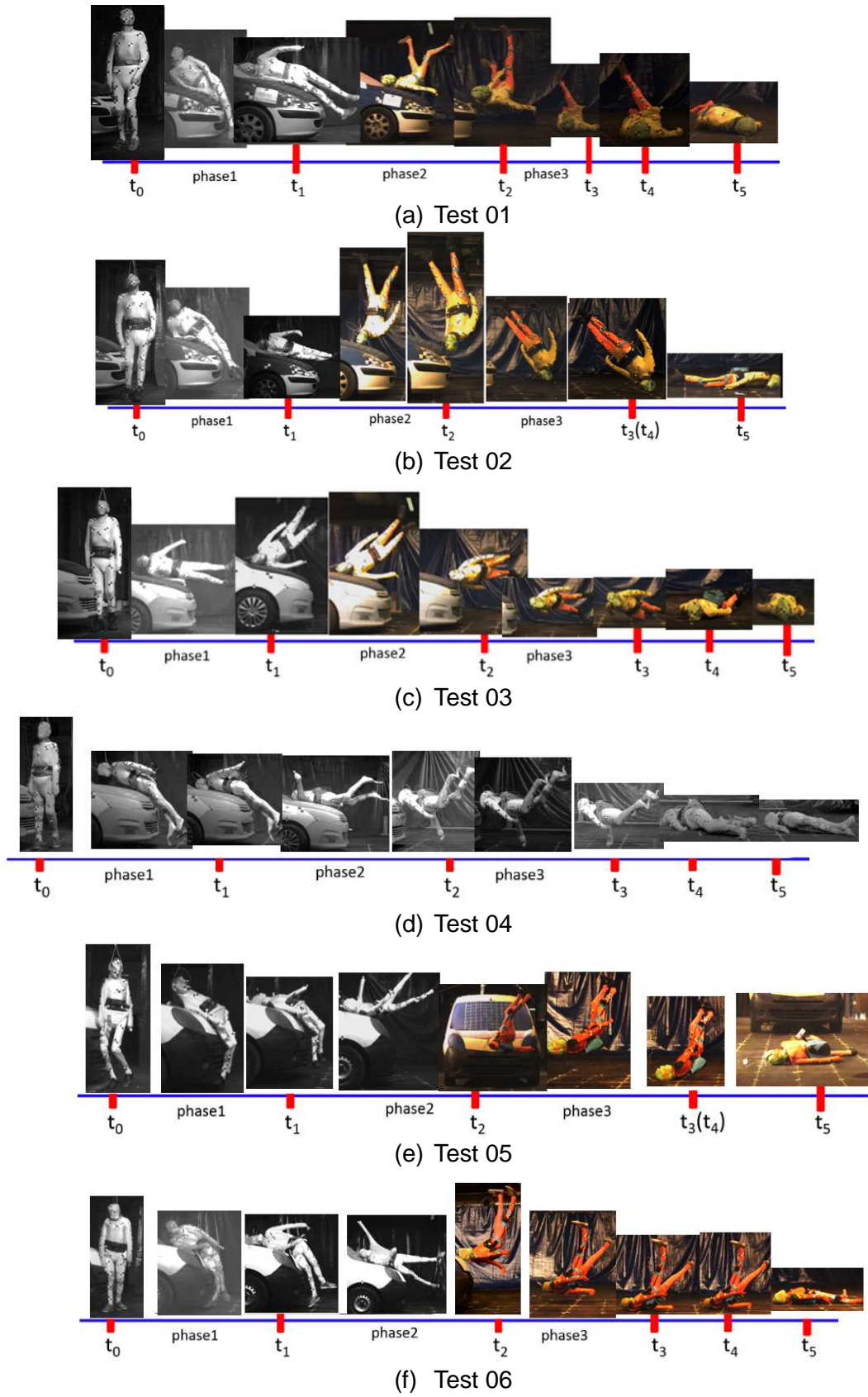
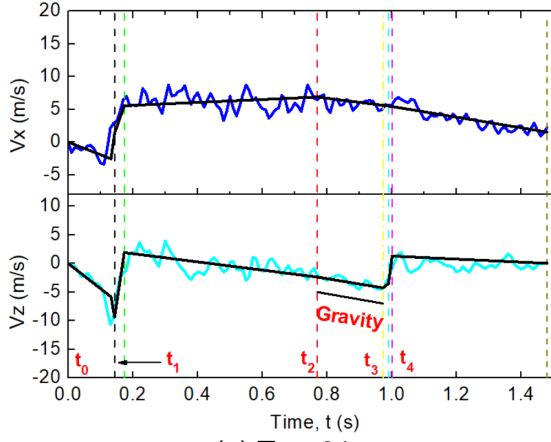


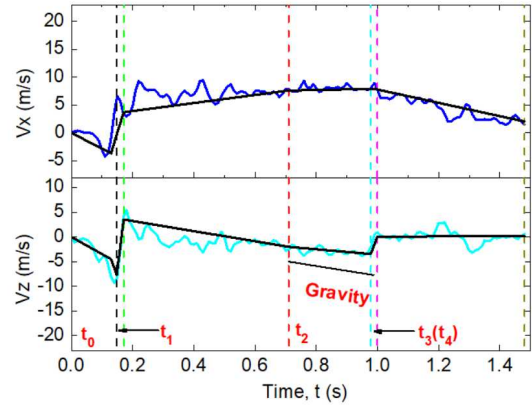
Figure 2: Sequences of vehicle-pedestrian impact for the six cadaver tests

The vehicle contact phase has been previously well documented (Kerrigan et al., 2007; Subit et al., 2008). Instead, our focus is on the subsequent ground contact. Following t_1 (first head contact on the vehicle, which occurs in all tests except Test 03 where shoulder contact & low impact speed prevent direct head contact), there is continued interaction of the pedestrian with the bonnet/windscreen area for about 500ms until separation commences. Figure 3 shows velocity changes of the head during the impact process. To aid in understanding and motivated by the principle of conservation of momentum, straight line approximations of the head linear velocity have been added to Figure 3, showing that no significant impacts occur between head contact on the vehicle and separation from the vehicle. Following separation, the head acceleration is close to gravity. Contact with the ground is predominantly vertical, with small horizontal head velocity changes. Figure 4 shows the head resultant acceleration during the vehicle and ground contact phases. Unfortunately, the accelerometer recording for Test 06 was corrupted during ground contact. Furthermore, to address potential accelerometer vibration (mounted in the cadaver's mouths using expanding foam), we employed a low-pass filter prior to injury assessments. Based on previous studies (Kang and Xiao, 2008; SAE, 1995) and in order to achieve a reasonable agreement between the predicted velocity changes during both vehicle and ground contact derived from differentiated video positions and integrated accelerometer curves (see Appendix H), we chose a CFC120 filter (3dB cut-off frequency = 200Hz), see Figure 4. With reference to Appendix H, a higher or lower cut-off threshold than 200Hz resulted in respectively over/ under-prediction of the velocity change compared to the video-based estimates. The significance of this approach is further addressed in the Discussion.

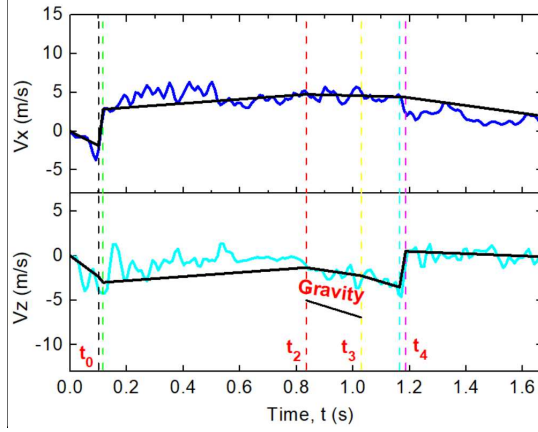
205
206
207



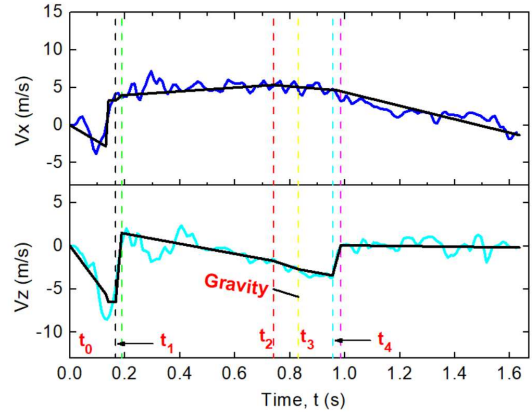
(a) Test 01



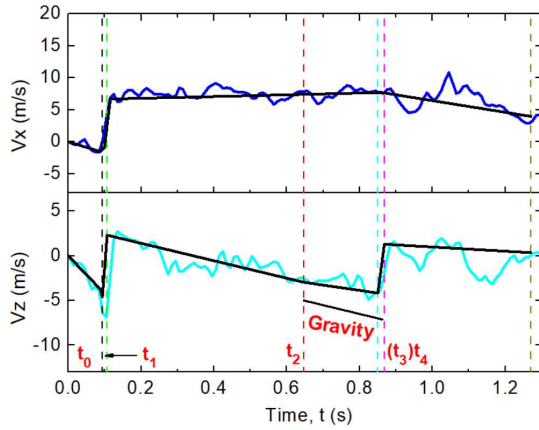
(b) Test 02



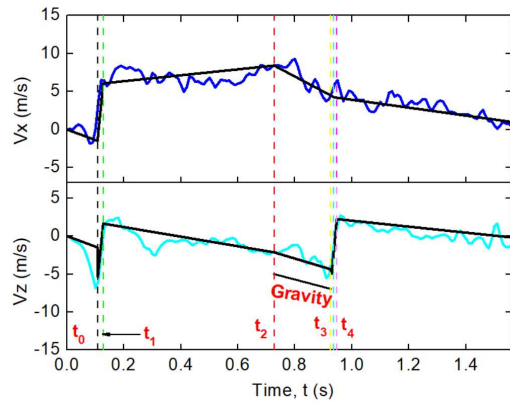
(c) Test 03



(d) Test 04



(e) Test 05



(f) Test 06

Figure 3: Head velocity time-histories from central difference (blue and cyan) with straight line approximations between major impact phases (black).

(Black dash: t_1 start; Green dash: t_1 end; Red dash: t_2 ; Yellow dash: t_3 ; Cyan dash: t_4 start; Purple dash: t_4 end)

208
209

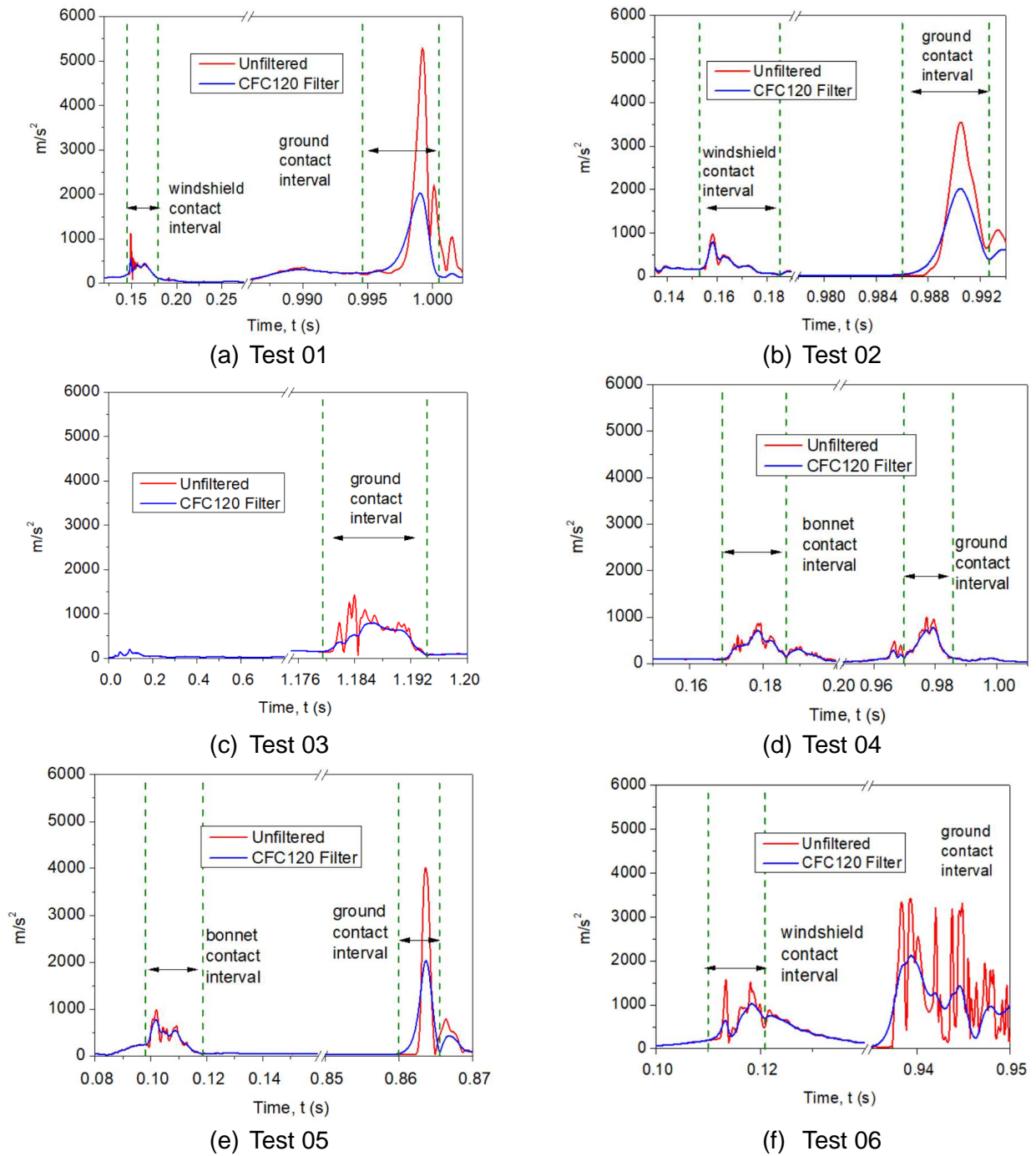


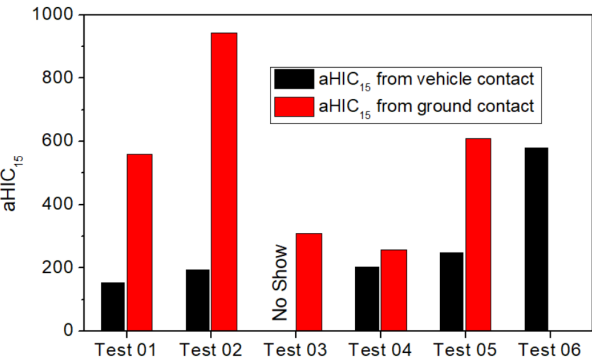
Figure 4: Filtered and unfiltered resultant head accelerometer time-histories during vehicle contact and ground contact

210

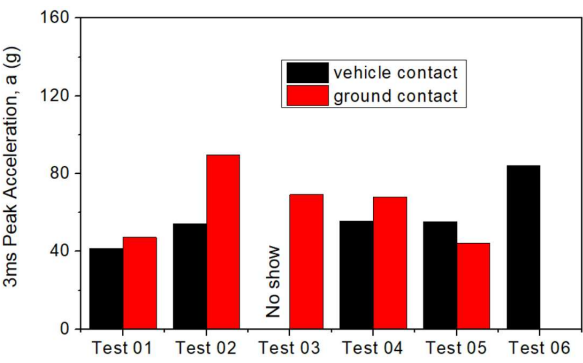
211

3.2 Head injury risk assessments

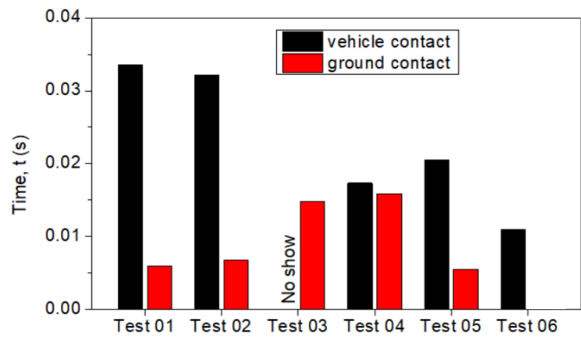
The *aHIC* scores for skull fracture risk based on the filtered acceleration curves for both vehicle and ground contacts are shown in Figure 5(a). **Erreur ! Source du renvoi introuvable.** The corresponding 3ms peak accelerations are shown in Figure 5(b), with head contact intervals in Figure 5(c). The *BrIC* score (including the range drive from the two independent MBIM estimates) and probabilities of AIS3+ brain injury risks are shown in Figures 5(d) & 5(e) respectively. A comparison of the variability in computed *BrIC* and linear velocity change scores between the two MBIM operators is given in Appendix I. Tables 3(a)&(b) summarize the vehicle and ground injury assessments. Figure 5(f) shows average ground related rotational brain injury risk for 20km/h and 30km/h cases. Table 3(c) compares the expected and actual ground impact “mechanisms” using the categories of (Crocetta et al., 2015), while Table 3(d) compares the corresponding head impact speeds. The “agreement” in Table 3(c) is based on the proposed “mechanisms” obtained from a previous simulation study (Crocetta et al., 2015). For pedestrian collisions from a compact car at 20 kph, almost all predicted cases were “M2”. For pedestrian collisions with a compact car or big car or SUV at 30 kph, the most frequently predicted mechanism was M1. If the mechanism observed from the cadaver test meets the most frequent mechanism from Crocetta et al, the “agreement” in Table 3(c) was categorised as “Yes”. If the observed mechanism was one of the less frequently predicted ones, the agreement was “Partial”. If the observed mechanism was not predicted, then the agreement was “No”.



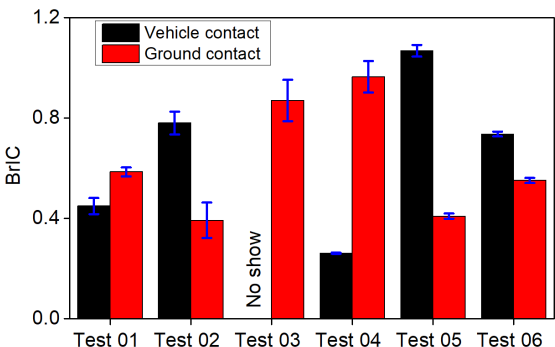
(a) Vehicle and ground related $aHIC$ scores



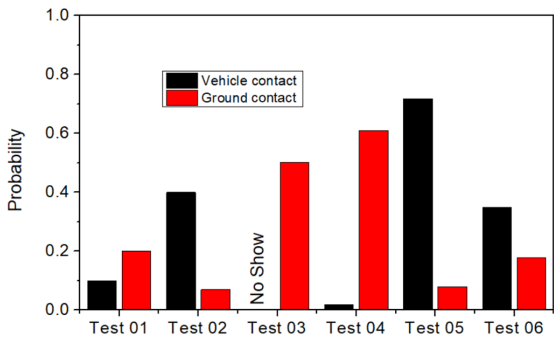
(b) The 3 ms head acceleration peaks



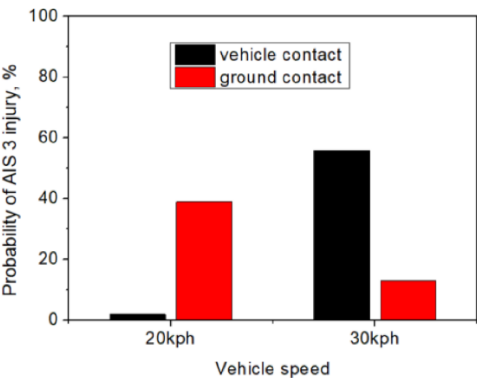
(c) Head contact intervals



(d) $BrIC$ scores



(e) Probability of AIS3 brain injury



(f) Average ground related AIS3+ rotational brain injury risk for 20km/h and 30km/h case

Figure 5: Summary of head injuries for vehicle and ground contact

Table 3a: Summary of head/vehicle contact injury assessments

Test number	Impact speed (km/h)	NBLEH	aHIC ₁₅	3ms (g)	AIS3+ (from BrIC)
Test 01	30	0.7	152	41.5	10%
Test 02	30	0.7	194	54.4	40%
Test 03	20	0.9	---	---	--
Test 04	21	0.9	203	55.5	2%
Test 05	30	1.2	248	55.3	72%
Test 06	30	1.1	579	84.1	35%

Table 3b: Summary of head/ground contact injury assessments

Test number	Impact speed (km/h)	NBLEH	aHIC ₁₅	3ms (g)	AIS3+ (from BrIC)
Test 01	30	0.7	559	47	20%
Test 02	30	0.7	943	90	7%
Test 03	20	0.9	309	69	50%
Test 04	21	0.9	258	68	61%
Test 05	30	1.2	608	44	8%
Test 06	30	1.1	--	---	18%

Table 3c: Expected and observed pedestrian ground contact mechanisms (Crocetta et al., 2015)

Test number	Expected	Actual	Agreement
Test 01	M1 (most frequent) or M3 (less frequent)	M1	Yes
Test 02	M1 (most frequent) or M3 (less frequent)	M3	Partial
Test 03	M2	M2	Yes
Test 04	M2	M2	Yes
Test 05	M2 (most frequent) or M1 (less frequent)	M1	Partial
Test 06	M2 (most frequent) or M1 (less frequent)	M1	Partial

Table 3d: Expected and observed ground contact speeds (Crocetta et al., 2015)

Test number	Cadaver head velocity (m/s) at ground contact	Average \pm std dev. head velocity (m/s) at ground contact from multibody predictions (Crocetta et al., 2015)
Test 01	5.1	4.7 \pm 0.8
Test 02	2.6	2.9 \pm 0.6
Test 03	5.1	3.2 \pm 1.4
Test 04	3.9	3.2 \pm 1.4
Test 05	4.4	4.7 \pm 0.8
Test 06	5.5	4.7 \pm 0.8

239 **4.Discussion**

240 ***Whole-body kinematics during the complete pedestrian impact process***

241 We present the first detailed overview of the kinematic process of pedestrian ground contact
 242 using cadavers (see Table 2 and Figure 2). The very limited previous data on pedestrian ground
 243 contact from cadaver tests limits comparison to the published literature. Whole body kinematics can
 244 be classified into several critical events and phases: phase 1 (duration ~100-170ms) starts with first
 245 pedestrian-vehicle contact and ends with first head-vehicle contact; in phase 2 (duration ~550-
 246 625ms) the pedestrian moves together with the vehicle; phase 3 (duration ~185-280ms) is
 247 separation and first pedestrian ground contact; phase 4 (duration ~1-1.8s) is slide, roll and bounce
 248 to rest. First head ground contact occurs after about 1s and the process is complete after about 2.0-
 249 2.8s. Pedestrian ground contact occurs at the end of a highly non-linear chain of events, such that
 250 small changes in initial configuration result in significant changes in head ground impacts (compare
 251 Test 01 to Test 02) and this has been well flagged in the literature (Simms and Wood, 2009).
 252 However, considering the ground contact “mechanisms” proposed by (Crocetta et al., 2015) – see
 253 Appendix C, surprisingly good agreement was observed (Table 3c) and head velocity prior to ground
 254 contact was similar to the range presented for each mechanism except for Test 03 (Table 3d). These
 255 results show multibody modelling is generally successful at predicting whole body motion of
 256 pedestrians during ground contact. Nonetheless, given variations in head ground impact observed
 257 in similar cadaver tests (especially Test 01 vs Test 02), the capacity to predict injury risk in specific
 258 ground contact cases is low, as per modelling observations (Li et al., 2017b).

259 ***Head kinematics throughout the impact process***

260 Head velocity changes (Figure 3) clearly identify the head/vehicle and head/ground contact
 261 processes. It is instructive to conceive of the head velocity changes in terms of net forces acting
 262 vertically and horizontally: the horizontal head velocity changes in phase 1 are due to neck forces
 263 induced during body rotation. Then there is the vehicle contact, after which the horizontal velocities
 264 during phases 2 and 3 are largely constant (almost zero net force) during separation from the
 265 vehicle through to first pedestrian ground contact, after which sliding and rolling to rest during phase
 266 4 reduce the horizontal velocity to zero. The vertical head velocity changes in phase 1 are again due
 267 to neck forces induced by body rotation. Then there is the vehicle contact, after which the vertical
 268 velocity changes approximately follow gravity during separation from the vehicle through to first
 269 pedestrian ground contact, which again effectively reduces the vertical component of head velocity
 270 to zero.

271 ***Head ground contacts***

272 The cadavers mostly struck the ground after around 1s (Test 05 was earlier but in this case
 273 there was an unusually low subject mass). The head impacts the ground more than once in each
 274 test, indicating significant restitution. However, estimates of head/ground contact stiffness using a
 275 spring-mass model with restitution were variable, between ca. 180-1750 kN/m, see Appendix J.
 276 Figure 3 shows that ground contact is predominantly vertical, with small horizontal velocity change
 277 during ground impact in all six tests. In contrast, the vertical velocity change during ground contact
 278 is chiefly responsible for the acceleration peaks in Figure 4. The peak accelerations, *aHIC* and *3ms*

279 scores from ground contact are generally higher than those from vehicle contact, see Figure 5. The
 280 high stiffness of the ground contact evidenced by the shorter contact interval compared to the
 281 vehicle contact (Figure 5c) is probably the main reason for this, since Appendix H shows the speed
 282 change in the vehicle contacts is mostly higher than in the ground contacts. This highlights the need
 283 to find solutions to pedestrian ground contact injury for pedestrian protection at impact speeds of 20
 284 - 30 km/h, where further improvements in vehicle front safety may be less beneficial than
 285 approaches to preventing pedestrian ground contact. These results are in line with our recent
 286 GIDAS analysis which found 72% of injury costs in pedestrian collisions below 30km/h are
 287 associated with ground related injuries (Shang et al., 2018b).

288 **Head accelerometer filtering**

289 According to the X-ray after each test, there were no skull fractures. This provides further
 290 justification for the 200 Hz filter, as the peaks in the unfiltered accelerations in Figure 4 would almost
 291 certainly imply some skull fractures. In addition, a retrospective assessment of the GIDAS data
 292 analyzed for the work published in (Shang et al., 2018b) shows the proportion of crashes involving
 293 skull fracture from ground contact is less than 4% in the speed range 25-34 km/h and less than 1%
 294 in the speed range 15-34 km/h, which also complies with the absence of skull fractures in our
 295 cadaver tests.

296 **Head linear versus rotational loading during ground contact**

297 A comparison of the relationship between *aHIC*/3ms linear head injury risk with the rotationally
 298 assessed AIS3+ risk computed from the *BrIC* score shows mixed results, see Figure 6. The *aHIC*
 299 score reduces with increased AIS3+ rotational head injury risk suggesting a compensatory pattern
 300 between head linear and angular injury risk which might depend on the geometry of head ground
 301 contact, but this pattern is not replicated for the 3ms score. It is thus unclear how to interpret these
 302 results and computational modelling may be needed to further elucidate this.

303

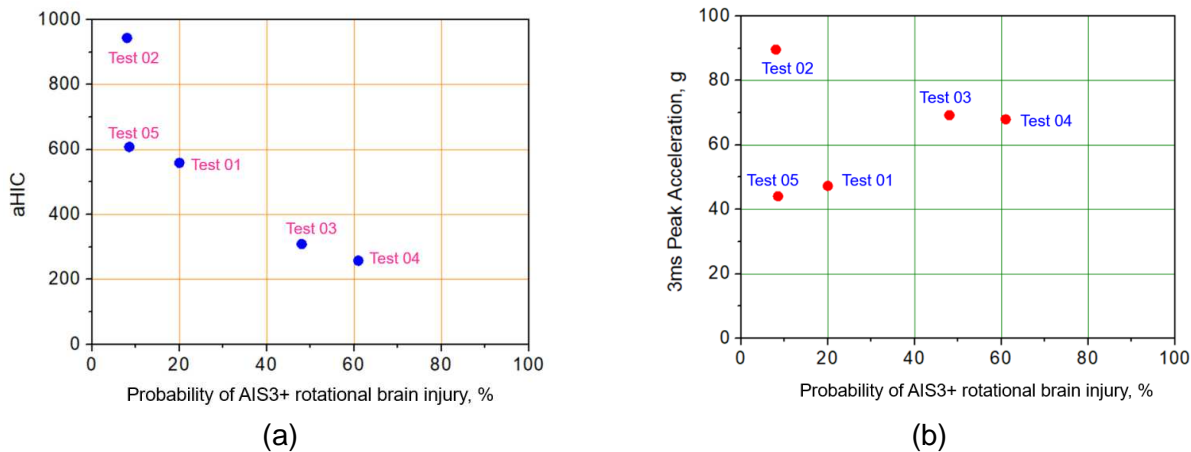


Figure 6: Comparison of the relationship between *aHIC*/3ms linear head injury risk with the rotationally assessed AIS3+ risk for Test 01-05 (the accelerometer malfunctioned in the ground contact in Test 06)

Unexpected Results

There were a number of unexpected findings that may lead to future insights:

Figure 5(f) and Table 3b show a substantially higher risk of rotationally induced brain injury for the two 20 km/h tests than the four 30 km/h cases. The reason for this is the combination of a larger ω_z component with the smaller threshold for this axis in the BrIC equation. By checking the head-ground contact mechanisms from the videos, the motion of the pedestrian heads in tests 03 and 04 was more complex (bending and twisting). In contrast, for the other tests, the heads showed mainly bending rotation during contact with the ground. An underlying biomechanical explanation and whether this predicted increased risk at 20kph occurs in real world collisions remains unclear, but future computational modelling may help elucidate this.

We had expected to identify a relationship between NBLEH and head injury risk as this was observed in our recent analysis of GIDAS data (Shang et al., 2018b), but Table 3a shows no clear relationship between either linear or rotational head injury risk assessments in ground contact and the NBLEH in our cadaver tests. The absence of a trend may be due to the small sample size.

5. Limitations

A larger sample size would be needed to better understand the influence of vehicle design and pedestrian ground contact. However, the current experimental findings could be combined with computational modelling to better understand these effects. Additional high-speed cameras and markers on the head would have been beneficial for the MBIM process, as the region of interest to be covered during the whole process from first contact to rest is large.

The CFC 120 filter applied to the accelerations gave the closest speed change by comparison with the MBIM data than any other filter we investigated, and we therefore believe it is appropriate to apply this filter setting. However, we acknowledge this filter not only reduces the peak but can also slightly change the contact time defined, see Figure 4. In future, a study dedicated to establishing appropriate filters for pedestrian ground contact would be helpful.

The accuracy of the angular velocity time histories derived from the MBIM process cannot be measured as there is no gold standard, and this is a limitation. However, compared to (Tierney et al., 2018), we expect a higher accuracy as the frame rate is higher and there are four cameras instead of three and the image resolution is better. The intraclass correlation coefficients for the results of the two independent researchers applying MBIM are given in Table I.1. An assessment of rotationally induced brain injury which includes a measure of angular acceleration would be preferable, however, unfortunately we were not able to estimate angular acceleration in this study due to limitations in the available sensors. Furthermore, we recognise the limitations of BrIC which include a lack of validation data and its possible weakness for predicting more severe injuries.

A nine accelerometer array suitable for computing head CG accelerations would have permitted more precise 3ms, HIC calculations and would also facilitate UBrIC computation. A method for enforcing known initial limb angles would be beneficial, but also difficult to achieve in these cadaver tests. Furthermore, the cadavers' lack of muscle tone may result in different kinematics compared to live pedestrians, especially for the two 20 kph tests. In this paper only head kinematics are presented, but the GIDAS data (Shang et al., 2018b) shows lower limb and spinal injuries also occur during pedestrian ground contact and these should be a focus of future work.

6. Conclusions

This paper presents the first detailed analysis of pedestrian ground contact kinematics using staged cadaver tests addressing a range of vehicle shapes and pedestrian heights and impact speeds of 20 and 30 km/h. In addition to the well-established kinematics of pedestrians up to the time of head contact on the vehicle, we have observed around 500 ms of continued interaction of the pedestrian on the vehicle until separation commences, followed by a flight period of around 200 ms which terminates in ground contact. The linear accelerations in ground contact for vehicle impact speeds of 20 and 30 km/h are generally higher than the acceleration in the vehicle contact, though the contact intervals are shorter. No skull fractures were observed in any cases, but the 3ms scores are close to or above the injury threshold in several cases. The predicted risk of rotationally induced brain injury computed from model based image matching applied to ground contact is high for the 20 km/h tests, highlighting the risk of pedestrian injuries from ground contact even at very low speeds. We were unable to identify a clear relationship between vehicle shape/pedestrian height and ground contact head injury risk in these six tests. The data pertaining to these six pedestrian ground contact tests can be made available upon request for the purpose of human body model development.

Conflict of Interest

The authors have no conflict of interest related to the present work to disclose.

Acknowledgement

The support of the China Scholarship Council (CSC) is highly appreciated.

References

- Aomura, S., Zhang, Y., Nakadate, H., Koyama, T., Nishimura, A., 2016. Brain injury risk estimation of collegiate football player based on game video of concussion suspected accident. *Journal of Biomechanical Science Engineering* 11, 16-00393-00316-00393.
- Ashton, S., Mackay, G., 1983. Benefits from changes in vehicle exterior design—field accident and experimental work in Europe. SAE Technical paper.
- Badea-Romero, A., Lenard, J., 2013. Source of head injury for pedestrians and pedal cyclists: Striking vehicle or road? *Accident Analysis & Prevention* 50, 1140-1150.
- Bahr, R., Krosshaug, T., 2005. Understanding injury mechanisms: a key component of preventing injuries in sport. *British Journal of Sports Medicine* 39, 324-329.
- Cavallero, C., Cesari, D., Ramet, M., Billault, P., Farisse, J., Seriat-Gautier, B., Bonnoit, J., 1983. Improvement of pedestrian safety: influence of shape of passenger car-front structures upon pedestrian kinematics and injuries: evaluation based on 50 cadaver tests. SAE Technical Paper.
- Crocetta, G., Piantini, S., Pierini, M., Simms, C., 2015. The influence of vehicle front-end design on pedestrian ground impact. *Accident Analysis & Prevention* 79, 56-69.
- ECE, 2008. Regulation No 21 of the Economic Commission for Europe of the United Nations (UN/ECE) — Uniform provisions concerning the approval of vehicles with regard to their interior fittings.
- ECE, 2010. Regulation No 25 of the Economic Commission for Europe of the United Nations (UN/ECE) —

387 Uniform provisions concerning the approval of head restraints (headrests), whether or not incorporated in
388 vehicle seats.

389 Gabler, L.F., Crandall, J.R., Panzer, M.B., 2016. Assessment of kinematic brain injury metrics for predicting
390 strain responses in diverse automotive impact conditions. *Annals of Biomedical Engineering* 44, 3705-3718.

391 Gabler, L.F., Crandall, J.R., Panzer, M.B., 2018. Development of a metric for predicting brain strain responses
392 using head kinematics. *Annals of Biomedical Engineering* 46, 972-985.

393 Goodarzi, N., Akbari, G., Razeghi Tehrani, P., 2017. Zinc Chloride, A new material for embalming and
394 preservation of the anatomical specimens. *Anatomical Sciences Journal* 14, 25-30.

395 Got, C., Patel, A., Fayon, A., Tarriere, C., Walfisch, G., 1978. Results of experimental head impacts on
396 cadavers: the various data obtained and their relations to some measured physical parameters. SAE
397 Technical Paper.

398 Gupta, V., Kalra, A., Shen, M., Chou, C.C., Yang, K.H., 2015. Effect of vehicle front end profile on pedestrian
399 kinematics and biomechanical responses using a validated numerical model, ASME 2015 International
400 Mechanical Engineering Congress and Exposition. American Society of Mechanical Engineers.

401 Gupta, V., Yang, K.H., 2013. Effect of vehicle front end profiles leading to pedestrian secondary head impact
402 to ground. SAE Technical Paper.

403 Hamacher, M., Eckstein, L., Kühn, M., Hummel, T., 2011. Assessment of active and passive technical
404 measures for pedestrian protection at the vehicle front, 22st International Technical Conference on the
405 Enhanced Safety of Vehicles (ESV 2011).

406 Han, Y., Li, Q., Wang, F., Wang, B., Mizuno, K., Zhou, Q., 2018. Analysis of pedestrian kinematics and ground
407 impact in traffic accidents using video records. *International Journal of Crashworthiness*, 1-10.

408 Hutchinson, J., Kaiser, M.J., Lankarani, H.M., 1998. The head injury criterion (HIC) functional. *Applied*
409 *Mathematics Computation* 96, 1-16.

410 Kalra, A., Gupta, V., Shen, M., Jin, X., Chou, C.C., Yang, K.H., 2016. Pedestrian safety: an overview of
411 physical test surrogates, numerical models and availability of cadaveric data for model validation. *International*
412 *Journal of Vehicle Safety* 9, 39-71.

413 Kang, S., Xiao, P., 2008. Comparison of Hybrid III rigid body dummy models, 10th International LSDYNA
414 Users Conference.

415 Kendall, R., Meissner, M., Crandall, J., 2006. The causes of head injury in vehicle-pedestrian impacts:
416 comparing the relative danger of vehicle and road surface. SAE Technical paper.

417 Kerrigan, J.R., Crandall, J.R., Deng, B., 2007. Pedestrian kinematic response to mid-sized vehicle impact.
418 *International Journal of Vehicle Safety* 2, 221-240.

419 Kimpara, H., Iwamoto, M., 2012. Mild traumatic brain injury predictors based on angular accelerations during
420 impacts. *Annals of Biomedical Engineering* 40, 114-126.

421 Li, G., Lyons, M., Wang, B., Yang, J., Otte, D., Simms, C., 2017a. The influence of passenger car front shape
422 on pedestrian injury risk observed from German in-depth accident data. *Accident Analysis & Prevention* 101,
423 11-21.

424 Li, G., Yang, J., Simms, C., 2017b. Safer passenger car front shapes for pedestrians: A computational
425 approach to reduce overall pedestrian injury risk in realistic impact scenarios. *Accident Analysis & Prevention*
426 100, 97-110.

427 Masson, C., Serre, T., Cesari, D., 2007. Pedestrian-vehicle accident: Analysis of 4 full scale tests with PMHS,
428 20th International Technical Conference on the Enhanced Safety of Vehicles (ESV) National Highway Traffic
429 Safety Administration.

430 Mueller, B., MacAlister, A., Nolan, J., Zuby, D., 2015. Comparison of HIC and BrIC head injury risk in IIHS

frontal crash tests to real-world head injuries, Proceedings of the 24th International Technical Conference on the Enhanced Safety of Vehicles.

Niebuhr, T., Junge, M., Rosén, E., 2016. Pedestrian injury risk and the effect of age. *Accident Analysis & Prevention* 86, 121-128.

Paas, R., Masson, C., Davidsson, J., 2015. Head boundary conditions in pedestrian crashes with passenger cars: six-degrees-of-freedom post-mortem human subject responses. *International Journal of Crashworthiness* 20, 547-559.

Rosen, E., Stigson, H., Sander, U., 2011. Literature review of pedestrian fatality risk as a function of car impact speed. *Accident Analysis & Prevention* 43, 25-33.

SAE, 1995. Instrumentation for impact test—Part 1—Electronic instrumentation. SAE 211.

Schmitt, K.-U., Niederer, P., Muser, M., Walz, F., 2010. *Trauma Biomechanics*. Springer.

Shang, S., Li, G., Otte, D., Simms, C., 2018a. An inverse method to reduce pedestrian - ground contact injuries IRCOBI Asia 2018.

Shang, S., Otte, D., Li, G., Simms, C., 2018b. Detailed assessment of pedestrian ground contact injuries observed from in-depth accident data. *Accident Analysis & Prevention* 110, 9-17.

Simms, C., 2005. Sports utility vehicles and older pedestrians. *BMJ* 331, 787.

Simms, C., Wood, D., 2009. *Pedestrian and Cyclist Impact*. Springer Netherlands.

Subit, D., Kerrigan, J., Crandall, J., Fukuyama, K., Yamazaki, K., Kamiji, K., Yasuki, T., 2008. Pedestrian-vehicle interaction: kinematics and injury analysis of four full scale tests, Proceedings of IRCOBI Conference, pp. 275-294.

Takhounts, E.G., Craig, M.J., Moorhouse, K., McFadden, J., Hasija, V., 2013. Development of brain injury criteria (BrIC). SAE Technical Paper.

Tamura, A., Duma, S., 2011. A study on the potential risk of traumatic brain injury due to ground impact in a vehicle-pedestrian collision using full-scale finite element models. *International Journal of Vehicle Safety* 5, 117-136.

Tamura, A., Koide, T., Yang, K.H., 2014. Effects of ground impact on traumatic brain injury in a fender vault pedestrian crash. *International Journal of Vehicle Safety* 8, 85-100.

Taneda, K., Kondo, M., Higuchi, K., 1973. Experiment on passenger car and pedestrian dummy collision, Proceedings of the International Research Council on the Biomechanics of Injury conference. International Research Council on Biomechanics of Injury, pp. 231-239.

Tierney, G., Krosshaug, T., Wilson, F., Simms, C., 2015. An assessment of a novel approach for determining the player kinematics in elite rugby union players, Proceedings of the International Research Council on Biomechanics of Injury, pp. 180-181.

Tierney, G.J., Joodaki, H., Krosshaug, T., Forman, J.L., Crandall, J.R., Simms, C.K., 2018. Assessment of model-based image-matching for future reconstruction of unhelmeted sport head impact kinematics. *Sports Biomechanics* 17, 33-47.

Versace, J., 1971. A review of the severity index. SAE Technical Paper.

WHO, 2013. Global status report on road safety 2013: supporting a Decade of Action. World Health Organization.

Winckler, G., 1974. *Manuel d'anatomie topographique et fonctionnelle*. Masson.

Xu, J., Shang, S., Yu, G., Qi, H., Wang, Y., Xu, S., 2016. Are electric self-balancing scooters safe in vehicle crash accidents? *Accident Analysis & Prevention* 87, 102-116.

Table A.1-1 External anthropometry

Anthropometry	Test 01	Test 02	Test 03	Test 04	Test 05	Test 06
1 total height	174	172	167	167	157	163
2 eyes / ground height	166	161	162	155	147	153
3 acromion / ground height	149	144	145	137	121	141.5
4 elbow / ground height	116	110	109	106	97	110
5 iliac spine / ground height	95	94	91	91	84	95
6 trochanter / ground height	88	89	82	86	78	89.5
7 hauteur interligne genoux/sol	46	46	45	44.5	42	49
43 ankle height	6	8	7	10	5	8.5
44 a arm high circumference	27.5	31.5	31	25.3	18	28.5
44 b arm low circumference	26	28	28	24	17.5	27
48 a forearm high circumference	27	24	28.5	25	16.3	25.7
48 b forearm low circumference	19	19	20	19	12.5	18
49 hand length	20	18	19	18	13	20
36 thigh high circumference	42	46	46.5	40.5	33.5	47.5
37 thigh low circumference	35.5	38	39	36	27	39.5
38 knee circumference	37.5	38	36.5	37.5	33	37
39 calf circumference	30.5	31	29.5	30.5	20	29
40 ankle circumference	26	25	26.5	26.5	22.5	25
41 foot width	10	10	10.5	10.5	7	85
42 foot length	27.5	27	26.5	22.5	20	23
10 shoulder width	43	48	39.5	40.5	28.5	36
20 axillary thoracic width	36	35	31	39	27	34
23 thorax width under sternum	35	34	31	31.5	24	31

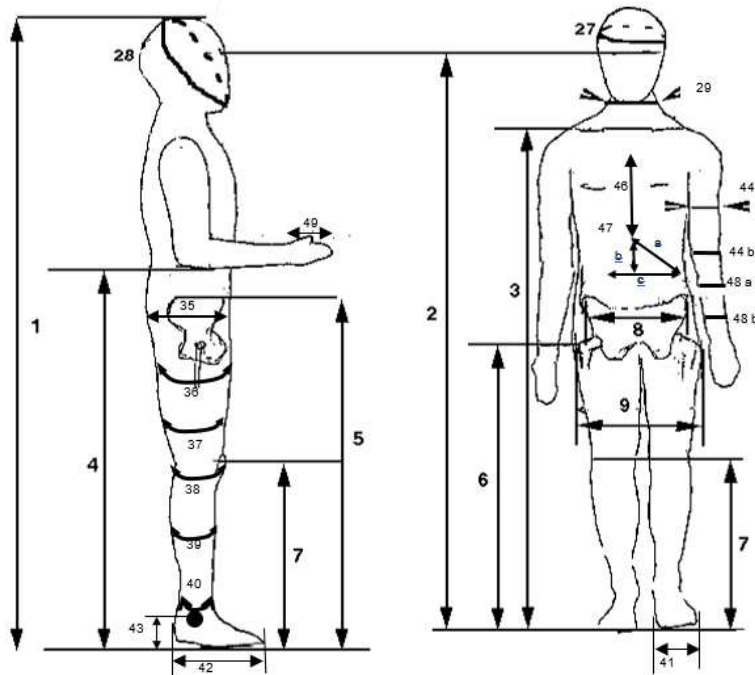


Table A.1-2 External anthropometry (continued)

Anthropometry	Test 01	Test 02	Test 03	Test 04	Test 05	Test 06
30 abdomen width	37	36	29	37	26	33
8 pelvis width	35	35	26.5	26	26.5	28
9 bi-trochanter width	39	36	39	33	27	36
21 thoracic axillary thickness	27	22	23	12	9	12
24 thoracic thickness under sternum	-	22	18	18	15	21
33 abdomen thickness	18	17	17	14	25.5	21
35 buttocks thickness	16	17	19	14	12	15
26a head / forehead depth	26	21	19	18	16	18
26b head height	28	23.5	20	21.5	20	23
26c head width	17.5	18	16	14	12	15
27 head circumference	55.5	58	56	56	52	56.5
28 chin-occipital circumference	72	69	63	59	62	61
29 neck circumference	41.5	48	40.5	39	33.5	48
18 forearm + hand length	46	44	37	41.5	34	44.5
19 arm length	33.5	32	32	32	26	30
10 seat height	98	88	85	92	72	85
11 eyes / seat height	90	77	80	83	62	75
14 cervical / seat height	79	70	70	68	55	67
12 acromion / seat height	73	60	63	65	48	63.5
13 elbow / seat height	40	16	27	33	26	37
22 axillary thoracic circumference	93	104	93	89	79	98
25 thoracic circumference under sternum	85	93	87.5	75	77	101
31 abdominal circumference (navel)	83	88	78	75	78	91
32 pelvis circumference	88	94	90	87	72	96
16 knee / ground height	46	51	51	43	41	48
17 buttocks / knee length	40.5	52	38	30	35	29
34 pelvis / heel (stretched leg) length	88	93	93	82	78	97.5
45 T1 – coccyx length	75	68	65	-	47	64
46 sternum length	17	19	19	22	19	20
47 xiphoid angle (a, b, c)	16 17 20	20 12 25	19 10 26	17 7 34	13 7 23	20 13 33

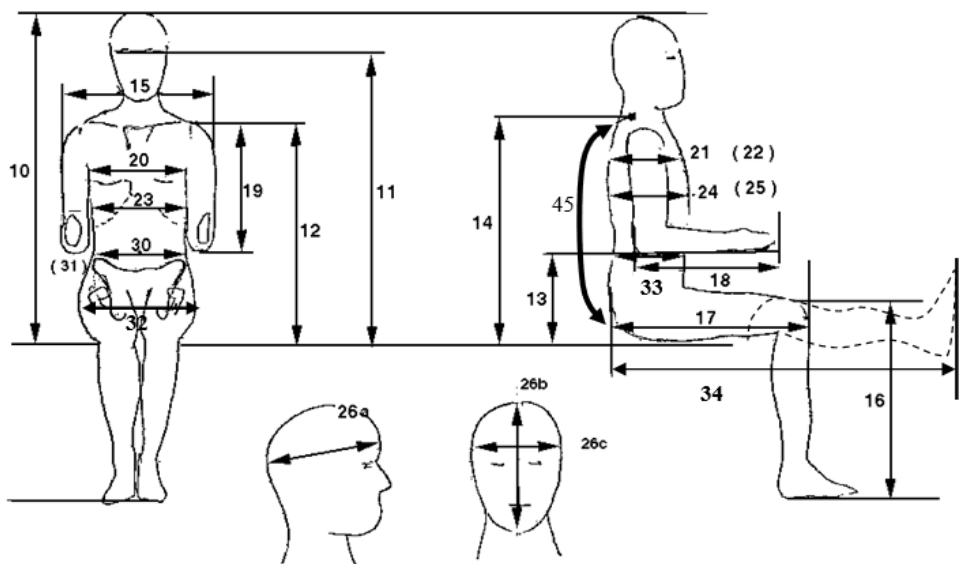



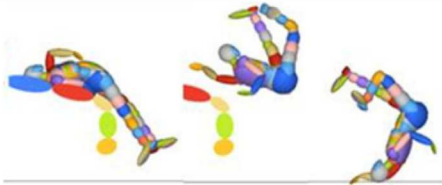

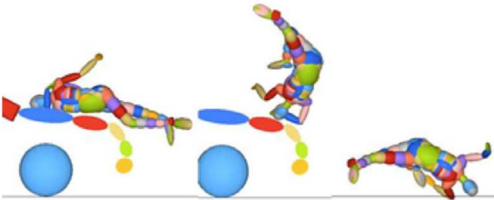


Table B1: Vehicles used

Vehicle model	Pictures of vehicle	Partly parameters of vehicle
(a) Peugeot 307	 A white Peugeot 307 hatchback with a blue and red sensor grid on the hood and windshield. The driver's side door is open.	Vehicle Height: 1510 mm Windshield Angle: 25.8 ° Bonnet Angle: 16.2° Bonnet length: 730 mm
(b) Citroen C4	 A white Citroen C4 hatchback with a yellow and blue sensor grid on the hood and windshield. The driver's side door is open.	Vehicle Height: 1491 mm Windshield Angle: 25.3° Bonnet Angle: 8.2° Bonnet length: 820 mm
(c) Renault Kangoo II	 A white Renault Kangoo II van with a blue and red sensor grid on the hood and windshield. The driver's side door is open.	Vehicle Height: 1844 mm Windshield Angle: 38.4° Bonnet Angle: 8.2° Bonnet length: 540 mm

487 **Appendix C: Ground contact “mechanisms”**
488

Table C1: Expected ground contact mechanisms (Crocetta et al., 2015)

Description	Kinematics
M1: wrap trajectory - pedestrian rotates 90°-180° before impacting ground head first	
M2: wrap trajectory - pedestrian rotates 0°-90° before impacting ground pelvis first, then head	
M3: wrap trajectory - pedestrian rotates 180°-270° before impacting ground head first	

489
490

491 **Appendix D: Camera layout used**
492

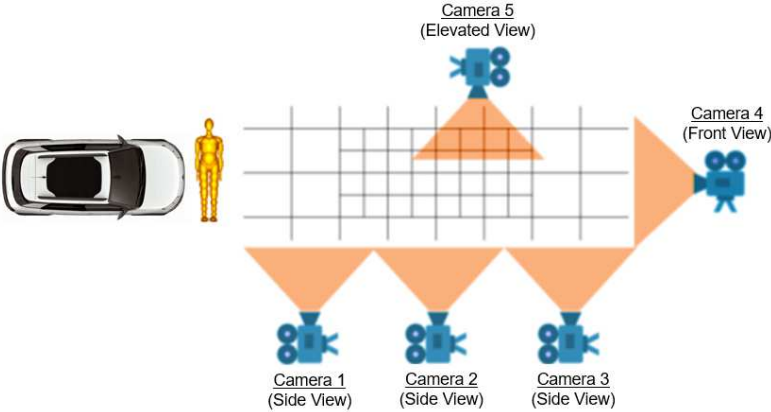


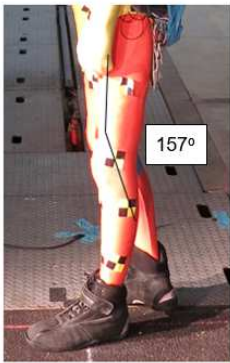
Figure D1: The general locations of the high-speed cameras

493
494
495

496 **Appendix E: Lower limb initial joint angles estimates**
497



(a) Test 01



(b) Test 02



(c) Test 03



(d) Test 04



(e) Test 05

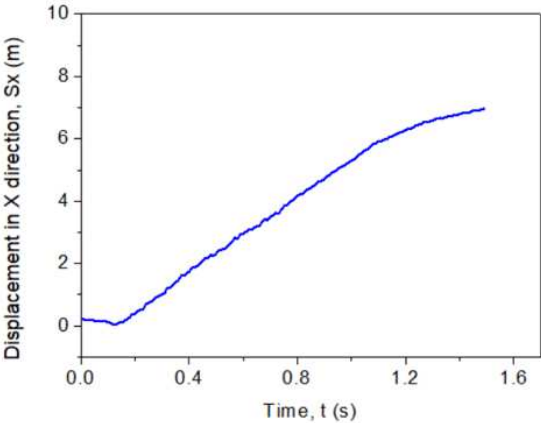


(f) Test 04

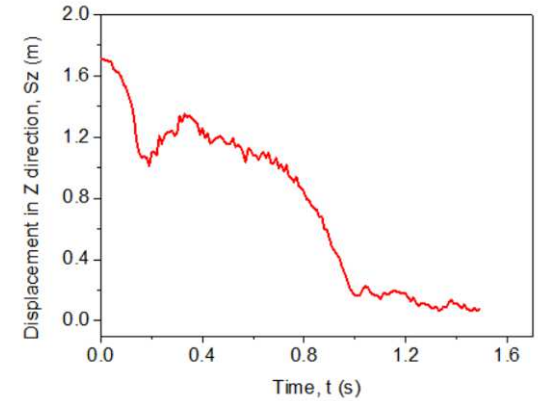
Figure E1: Knee joint angles in pre-impact positions

498
499
500

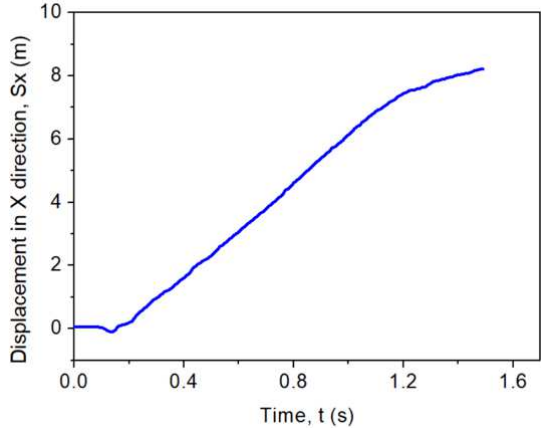
501 **Appendix F: Head marker trajectories in tests**
502



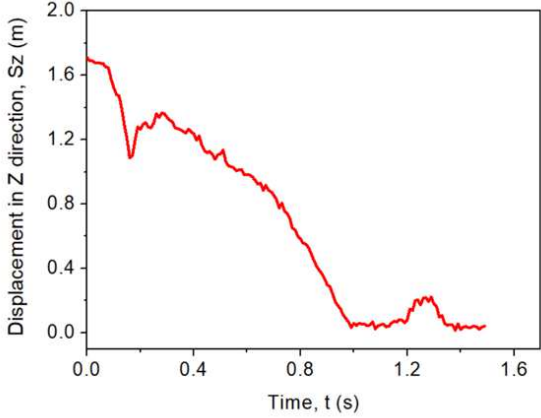
(a) Head position in X direction for Test 01



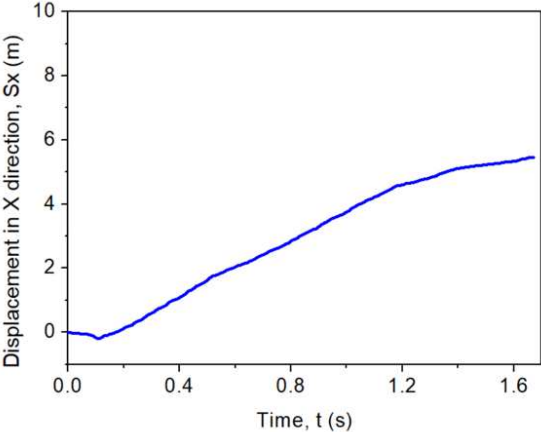
(b) Head position in Z direction for Test 01



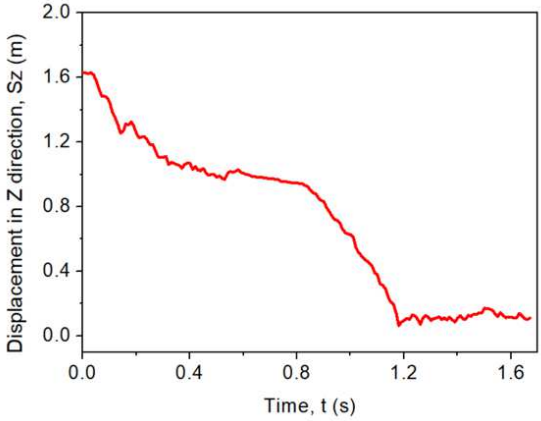
(c) Head position in X direction for Test 02



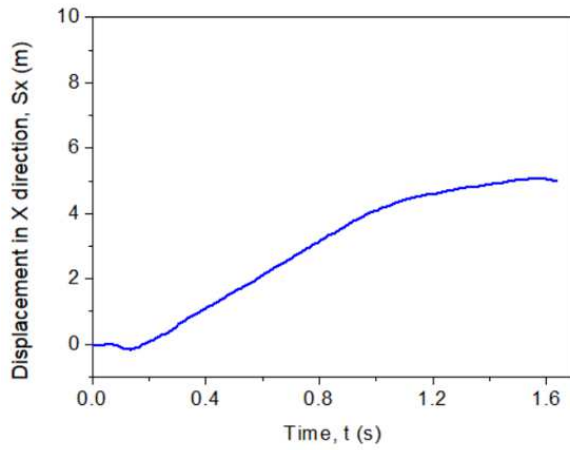
(d) Head position in Z direction for Test 02



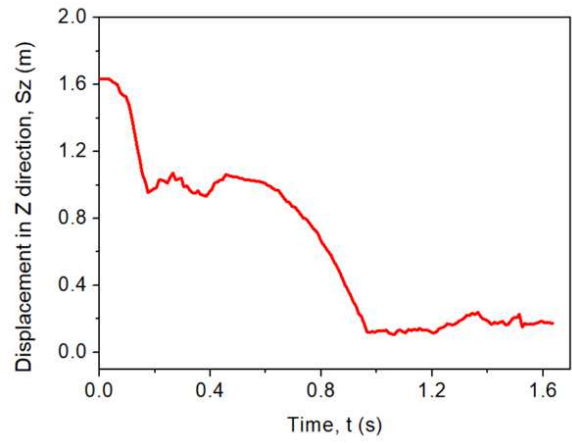
(e) Head position in X direction for Test 03



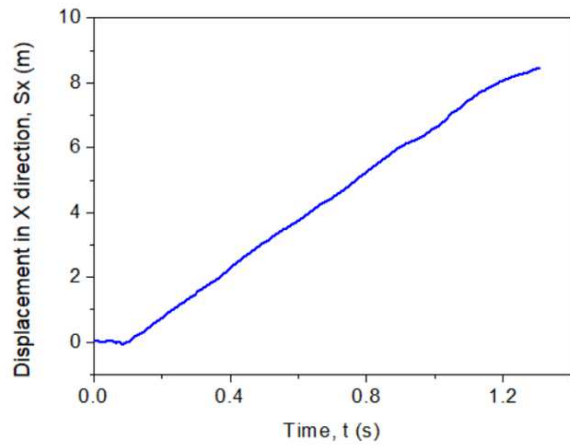
(f) Head position in Z direction for Test 03



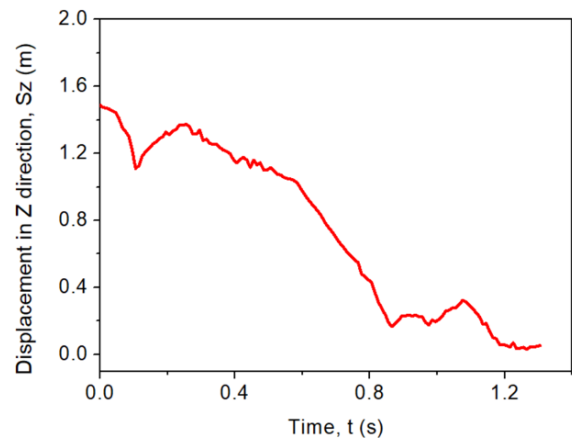
(g) Head position in X direction for Test 04



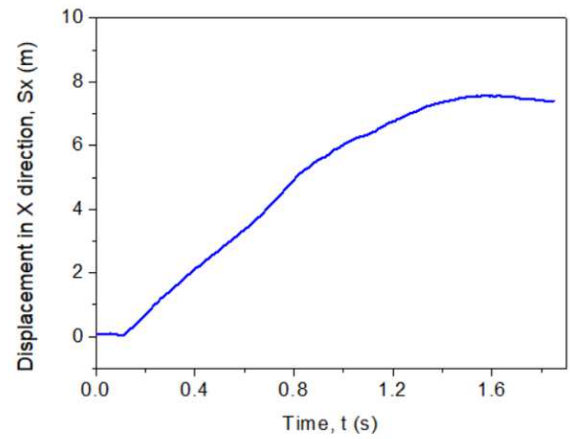
(h) Head position in Z direction for Test 04



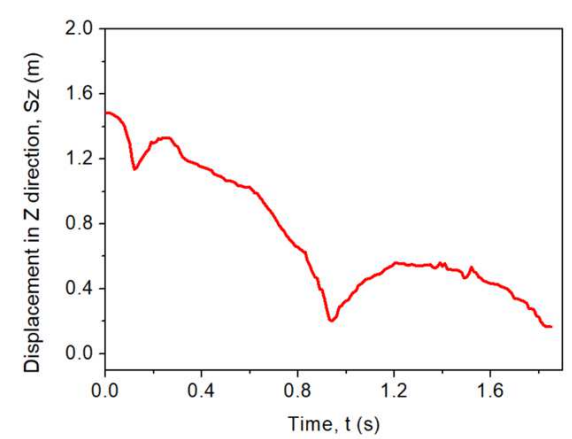
(i) Head position in X direction for Test 05



(j) Head position in Z direction for Test 05



(k) Head position in X direction for Test 06



(l) Head position in Z direction for Test 06

Figure F1: Cadaver head displacement in X and Z directions for the six tests

503
504
505

506 **Appendix G: Head impact location on vehicle**
507

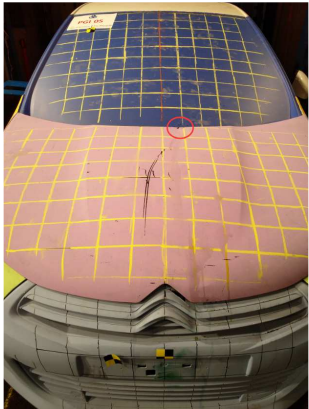


(a) Test 01



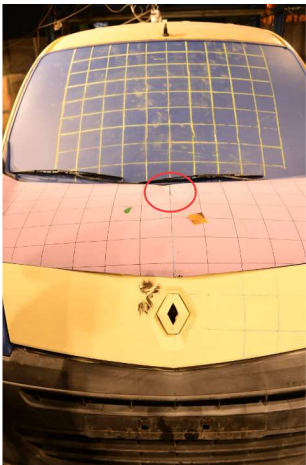
(b) Test 02

No head contact

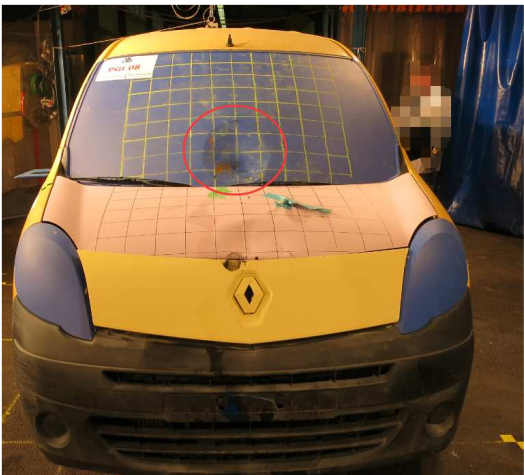


(d) Test 04

(c) Test 03



(e) Test 05



(f) Test 06

Figure G1: Pedestrian head impact location on vehicle

508

509 **Appendix H: Head resultant velocity change during vehicle and ground contacts from video**
510 **data differentiation and accelerometer integration**
511

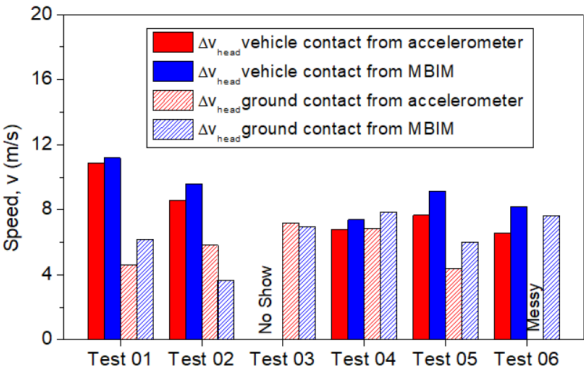


Figure H1: Comparison of head speed changes from MBIM and accelerometer

512

513

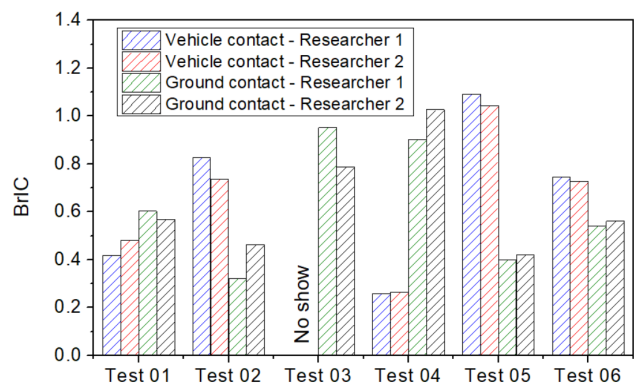


Figure I.1: Comparison of *BrIC* scores between researchers performing MBIM

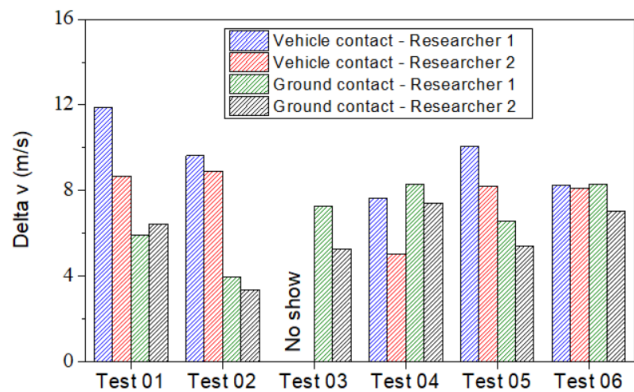


Figure I.2: Comparison of linear velocity changes between researchers performing MBIM

Table I.1-1: Intraclass correlation coefficients
for two independent MBIM researchers for vehicle contact

	Test 01			Test 02			Test 03			Test 04			Test 05			Test 06		
	Vehicle contact			Vehicle contact			Vehicle contact			Vehicle contact			Vehicle contact			Vehicle contact		
	Pos	Lin Vel	Ang Vel	Pos	Lin Vel	Ang Vel	Pos	Lin Vel	Ang Vel	Pos	Lin Vel	Ang Vel	Pos	Lin Vel	Ang Vel	Pos	Lin Vel	Ang Vel
X	0.928	0.335	0.844	0.995	0.325	0.945	NA	NA	NA	0.993	0.965	0.005	0.998	0.969	-1.402	0.998	0.567	0.984
Y	-0.048	0.95	NA	0.948	0.774	0.888	NA	NA	NA	-0.107	-0.371	0.981	0.749	0.901	0.967	0.749	0.64	NA
Z	0.992	0.98	NA	0.978	0.762	-0.015	NA	NA	NA	0.959	0.99	0.091	0.988	0.987	0.963	0.988	0.954	NA

Table I.1-2: Intraclass correlation coefficients
for two independent MBIM researchers for ground contact

	Test 01			Test 02			Test 03			Test 04			Test 05			Test 06		
	Ground contact			Ground contact			Ground contact			Ground contact			Ground contact			Ground contact		
	Pos	Lin Vel	Ang Vel	Pos	Lin Vel	Ang Vel	Pos	Lin Vel	Ang Vel	Pos	Lin Vel	Ang Vel	Pos	Lin Vel	Ang Vel	Pos	Lin Vel	Ang Vel
X	0.992	0.335	-0.124	0.998	0.325	0.36	0.975	0.937	-3.142	0.994	0.965	0.982	0.998	0.985	0.949	0.997	0.567	0.002
Y	0.977	0.95	0.05	0.969	0.774	0.691	0.877	0.582	0.906	0.582	-0.002	0.982	0.312	0.249	0.968	0.721	0.64	0.874
Z	0.995	0.98	0.919	0.938	0.762	0.933	0.996	0.649	0.841	0.964	0.99	0.929	0.971	0.99	-0.023	0.958	0.954	-0.061

Appendix J: Estimated head ground contact stiffness.

Table J1 shows the tests in which the ground contact mechanisms were suitable for estimating head ground contact stiffness. Consequently, Table J2 shows the reasons for the remaining tests.

Table J1: Contact location for suitable cadaver tests

Suitable Tests	Impact Location
Test 01	Occipital/parietal bone
Test 04	Chin
Test 05	Occipital/parietal bone

Table J2: Reasons for unsuitable cadaver tests

Unsuitable Tests	Reason
Test 02	Force goes through the head and head, preventing head rebound
Test 03	Facial padding adds damping
Test 06	Acceleration is not available

Table J.3 shows the head ground contact stiffness basing on the following equation and assuming a head mass (M) of 4.5kg:

$$k = \frac{M}{(\Delta t)^2} \left[\pi^2 + (Ine)^2 \right] ,$$

where e is the coefficient of restitution, which is defined as the rebound velocity divided by the velocity prior to contact. Values of pre/post impact velocity were taken from the MBIM results.

Table J.3: Head ground contact stiffness

Suitable Tests	Velocity before (m/s)	Velocity after (m/s)	e	Δt (ms)	k (kN/m)
Test 01	-5	0.75	0.15	5.9	1741
Test 04	-4	2.75	0.69	15.9	178
Test 05	-4.5	1.25	0.28	5.5	1709